Tribol Lett (2008) 29:185–192
DOI 10.1007/s11249-007-9295-9

ORIGINAL PAPER

Simulated Effects of Measurement Noise on Contact Measurements Between Rough and Smooth Surfaces

Caprice Gray · Robert White · Vincent P. Manno · Chris B. Rogers

Received: 4 October 2007 / Accepted: 27 December 2007 / Published online: 15 January 2008
© Springer Science+Business Media, LLC 2008

Abstract To test the accuracy of optically measuring contact, we examined the height distribution histogram of a simulated rough surface contacting a smooth surface. We qualified the technique sensitivity as a function of the inverse signal-to-noise ratio having values ranging from 0 to 0.3. An explanation of how the analysis technique can be applied to Dual Emission Laser-Induced Fluorescence (DELIF) measurements is provided.

Keywords Data acquisition · Contact mechanics · Polishing · Optical microscopy · Surface roughness · Measurement methods

1 Introduction

Contact between rough and smooth surfaces plays a leading role in several tribology applications including Chemical Mechanical Polishing (CMP) [1–4], therefore accurate measurements of contact are important. In silicon CMP, silicon wafers are planarized by the action of chemically active colloidal slurry and a micro-textured polishing pad, often made of polyurethane [1]. Through this polishing, the surface roughness of the raw silicon wafer can be reduced from hundreds of nanometers to tens of nanometers [5]. There is evidence that the pad–wafer friction signature changes as the surface roughness is reduced [6], a possible end-point detector of the polish flatness or completion of the material removal [7]. Understanding the amount of pad–wafer contact is an essential piece of the polishing mechanism puzzle, since many believe that contact is required for material removal [8, 9].

Contact is a difficult property to measure in a tribological system because most interfacing surfaces are opaque and difficult to access with sensors. While contact has been measured between opaque surfaces using ultrasonic measurements [10], the spatial resolution of such techniques is limited to just less than 1 mm. In order to observe micron-scale effects, such as single asperity contact, other optical methods, such as interferometry [11], confocal reflectance interference contrast microscopy (C-RICM) [12], and Dual Emission Laser-Induced Fluorescence (DELIF) [13] must be employed. These methods often require modifying one of the opaque surfaces with an optical window. DELIF and interferometry are 3D imaging techniques that require image analysis for asperity contact detection. When contact occurs, the asperity tips of the softer rough surface flatten. The resulting asperity contact area is often a very small portion of the image [L. Borucki, Private Communication, March 2007, 14] and as a result, imaging noise can lead to significant errors in contact detection.

Ex situ 3D interferometric images of CMP polishing pads have been analyzed using a histogram to plot the surface height distribution of the pad surface asperities after polishing [15]. While the focus of this work was to examine how diamond pad conditioners affected the asperity surface, it was also suggested that pad–wafer contact information can be extracted from these histograms by observing the surface height extreme [15]. As contact increases, the asperity tips will be compressed, resulting in greater uniformity of maximum asperity heights, illustrated in Fig. 1. A secondary peak arises in the surface height histogram at the maximum height extreme because the

C. Gray (✉) · R. White · V. P. Manno · C. B. Rogers
Department of Mechanical Engineering, Tufts University, 200 College Ave, Anderson Hall Room 204, Medford, MA 02155, USA
e-mail: caprice.gray@tufts.edu

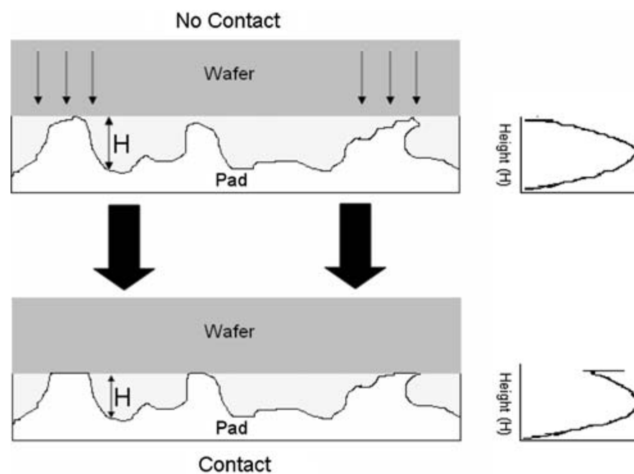

Fig. 1 When the wafer is not in contact with the pad, the height distribution of the pad surface as measured from the wafer surface has only a primary peak where the mean pad height is located. When the wafer is lowered, the pad asperities compress and a secondary peak arises at the height of the wafer

asperity heights have been equalized to the level of the wafer. The interferometer data reported in [15] were taken ex situ. Therefore, compressed asperities had time to rebound, making it difficult to extract a reliable measure of contact during polishing in situ. We would need to observe pad surface heights during polish (in situ), in the contacting environment in order to make realistic contact measurements.

The DELIF method provides a way of measuring contact information in situ [13]. DELIF is used to measure the fluid, i.e. slurry layer thickness, between the wafer and pad surfaces [16–18]. High-intensity (brighter) areas on a DELIF image represent valleys between asperities in which the fluid layer is the thickest. The fluid layer thickness goes to zero at contact, resulting in a dark area on the DELIF image. The fluid layer thickness can therefore be a quantitative measure of the asperity height distribution assuming that the contacting wafer is orders of magnitude smoother than the polishing pad.

Figure 2a shows a DELIF image of a Cabot Microelectronics D100 (CMC D100) polishing pad, and Fig. 2b shows the image intensity distribution for that surface. Since the intensity in Fig. 2a is representative of the slurry layer thickness, the dark portions of the image represent small amounts of slurry and asperity peaks whereas the light portions represent pores and valleys between asperities. The surface height distribution is nearly Gaussian for this region of the polishing pad (which is not true for all polishing pads). Note that Fig. 2b is a semi-log plot so as to emphasize the low-intensity extreme on the left side of the curve. Since contact in DELIF is observed when there is a greater count of dark pixels, this low-intensity extreme is where a secondary peak would arise due to pad–wafer contact. Theoretically, asperity height equalization due to contact should appear as a sharp peak, as in Fig. 1, in the low-intensity extreme, but the histogram in Fig. 2b only shows a smoothed secondary peak and an inflection point between the secondary and primary peak. The contact threshold for the images in [13] is chosen based upon the location of the infection point that separates the secondary from the primary peak. The sum of the area under the secondary peak, shaded in gray, is the contact percentage for the imaged region in Fig. 2a. This secondary peak is the only feature of the histogram that correlates to changes in applied pressure [13], which in turn implies that information about pad–wafer contact is contained in this region, since contact area must increase with increased pressure.

The lack of a sharp peak in the low-intensity extreme is likely due to imaging noise. Even though noise is an unavoidable characteristic of any measurement method, it is possible to extract accurate quantitative pad–wafer contact information from these histograms. In this article, we have simulated contact between a Gaussian surface and a flat surface with varying imposed measurement noise in order to demonstrate that accurate contact data can be extracted from DELIF images, as well as other 3D optical imaging techniques. In order to determine how reliable such a technique can be, we explored the impact of simulated imaging noise levels on the ultimate shape of the asperity height distribution curve, and quantify the resulting errors in measured contact percentage.

2 Simulation

We simulated a pad surface by placing randomly generated (Gaussian weighted) height values into a two-dimensional (512 $\times$ 696) array. The array size was chosen to match the dimensions of DELIF image data. The generated surface heights were normalized such that the highest asperities have a height value of 0, and the lowest valleys have a value of 1. Contact between this rough surface and a perfectly smooth flat surface was simulated by assuming the flat surface was located at a height (H) from the rough surface. All pixels in the rough surface with height values less than the flat surface threshold height were reassigned to be the flat surface threshold value as illustrated in Fig. 3. This is the equivalent of saying that every asperity is compressed within itself without expanding laterally. Although the pad material will expand under compression, we estimate the strain to be about 0.03 and therefore negligible, assuming Poisson's ratio for our surface is no greater than 0.1 [19]. Figure 3 is a cross section of the original Gaussian surface, which is shaded in dark gray. The smooth surface, shaded in light gray, is shown at a

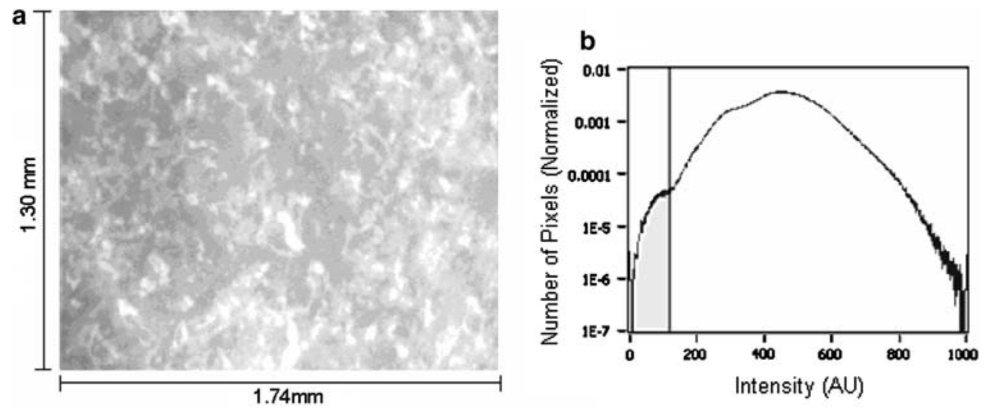

Fig. 2 (**a**) A typical DELIF image of a Cabot Microelectronics D100 polishing pad. Low intensity reflects portions of the image with little or no fluid and asperity peaks, whereas high intensity shows a thick fluid layer and valleys between asperities. (**b**) The intensity distribution for the DELIF image. The corresponding tallest asperities will be found on the left side of the graph in the low-intensity region

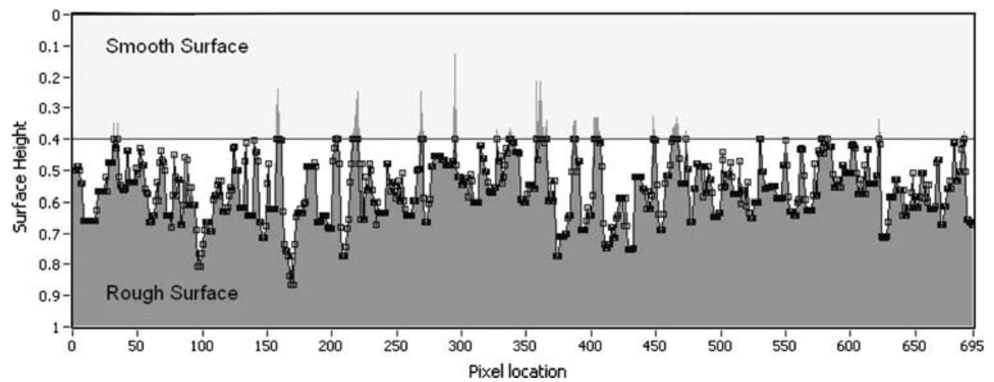

Fig. 3 A cross section of the rough-smooth surface contact for a smooth surface height $H = 0.4$. The Gaussian rough surface is shaded in dark gray, the smooth surface is light gray, and the contacting surface is outlined with the black boxed line

height, $H = 0.4$, in Fig. 3. A *real contact* percentage can be calculated from the contacting surface for various values of H. We define the *real contact* percentage as the contact that would be measured by a perfect measurement system with no significant noise. The *real contact* percentage is the number of pixels from the original Gaussian pad surface with height values above the height threshold, H, divided by the total number of pixels in the image:

$$\text{real contact\%} = \frac{\#\text{pixels} \geq H}{\text{total pixels in image}} \times 100 \tag{1}$$

The *real contact* percentages for the various H values discussed in this article are tabulated in Table 1.

A simulated measurement image was created by adding Gaussian noise to the contact image. The original Gaussian surface has a standard deviation, σ_1, and the noise added to the simulated contact surface has a standard deviation, σ_2. All simulated measurement images have an associated noise ratio, η, which is the ratio of the standard deviations,

$$\eta = \frac{\sigma_2}{\sigma_1} = \frac{\text{noise variation}}{\text{signal variation}} \tag{2}$$

We use the inverse of the signal-to-noise ratio, η, because we are simulating low noise values. For each value of H, measurement images were simulated with various values of η and the resulting effect on the histogram shape was observed. In Fig. 4, a histogram of the original contacting surface ($\eta = 0$) is compared to a simulated measurement image surface with $\eta = 0.1$ and $H = 0.225$. The contact region is illustrated in the histogram by a spike in the left-hand side of the distribution for the original contacting surface. Higher values of η result in a greater smoothing of the contact peak.

Table 1 *Real contact* percentages for the simulated rough-smooth surface contact for various smooth surface heights, H

Smooth surface height (H)	*Real contact* percentage	Contact estimate (%)	
		$\eta = 0.1$	$\eta = 0.2$
0	0	0.00036 ± 0.00014	0.00056 ± 0.00035
0.075	0.0025	0.0032 ± 0.0012	Undetectable
0.15	0.022	0.030 ± 0.017	Undetectable
0.225	0.31	0.39 ± 0.09	0.44 ± 0.28
0.3	2.2	2.4 ± 0.4	3.5 ± 0.7
0.4	14	13 ± 1	18 ± 1

The estimated contact for $\eta = 0.1$ and $\eta = 0.2$ are also tabulated

Once the histogram of the measurement image has been calculated, we can extract the contact percentage from the histogram and compare this measured percentage with the noise-free contact percentage. In order to extract the contact percentage from the histogram, we must isolate the subsection of the histogram extreme that contains the

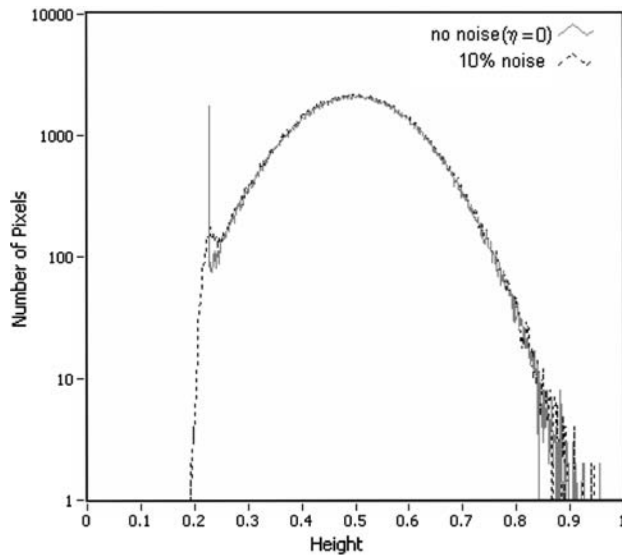

Fig. 4 The height distribution of the contacting surface (dashed-black) for a wafer height, $H = 0.225$, compared to a simulated measurement image with a noise ratio, $\eta = 0.1$

contact information. For this simulation, the left hand extreme of the histogram is isolated as shown in Fig. 5. The inflection point at the boundary of the primary and secondary peak can be distinguished by taking the local point-by-point derivative of the histogram subset near the secondary to primary peak transition and searching for the minimum value of the derivative. The derivative is calculated using a central difference on the histogram subsection:

$$\delta Y_i = \frac{(y_{i+1} - y_{i-1})}{2\delta x} \quad i = 1\ldots(n-1) \tag{3}$$

where δY_i are the values of the derivative, y_i are the histogram y-values, δx is the intensity (or height) difference between x-values on the histogram, and n is the total number of bins in the histogram subsection. The x-axis height value for the minimum point in the derivative is used as a contact threshold value for the asperity height distribution histogram. The contact percentage is estimated by calculating the ratio of the area to the left of the threshold to the area under the entire histogram. This quantification method is slightly dependent on the number of bins, n. For instance, the measured contact percentage for a simulated image in which the wafer is not in contact with the pad ($H = 0$) is 0.006% for a histogram with 200 bins, compared to 0.0007% for a histogram with 500 bins. This minor measurement error is a consequence of a measuring a larger range of intensities per bin when the level of discretization is lower. All data presented below were calculated using histograms discretized to 500 bins.

The histogram subset to be used in Eq. 3 is chosen by selecting the region around the wafer height within 2/3 of a standard deviation of the measurement noise: $H \pm (2/3\ \sigma_2)$. In order to reduce noise in the derivative, the original points in the histogram with coordinates x_i and y_i, are smoothed by a simple averaging low pass filter (Eq. 4) which generates the smoothed histogram coordinates, x_j and y_j, before the derivative is calculated.

$$x_j = \frac{\sum_{i=js}^{js+s} x_i}{s} \quad y_j = \frac{\sum_{i=js}^{js+s} y_i}{s} \tag{4}$$

where s is the smoothing factor, or number of points used to calculate the mean coordinate. Since increasing noise results in greater uncertainty in finding the inflection point, we increase the window size based on the value of η for each measurement image:

$$s = k\eta + 1 \tag{5}$$

where k is a constant which produces the best smoothing result. The value of s is rounded to the nearest integer. For this simulation we used a value of $k = 10$, which will yield a 3 point average smooth for $\eta = 0.2$. When there is little or no measurement noise ($s = 1$), the histogram will not be smoothed. The simulated surfaces are idealized and produce relatively smooth histograms requiring relatively low

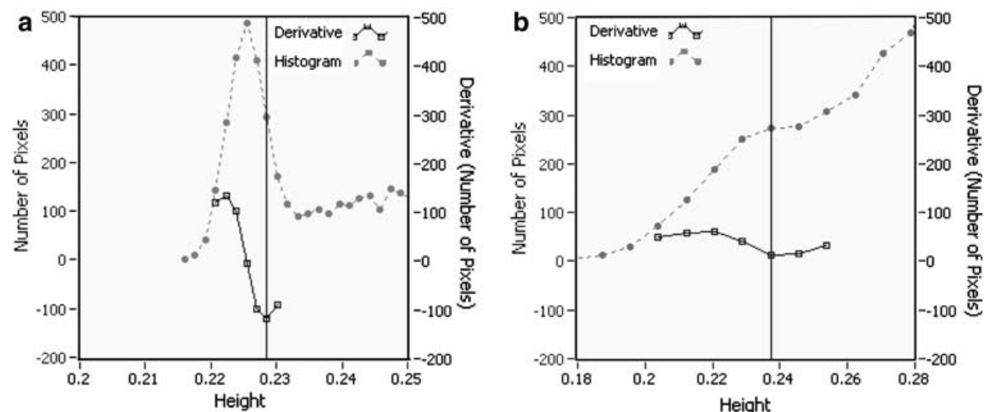

Fig. 5 The contacting extreme subsection of a measurement image histogram (gray) and the subsection derivative (black). The vertical line denotes the contact threshold as determined by the minimum value of the derivative. (**a**) $H = 0.225$, $\eta = 0.1$; (**b**) $H = 0.225$, $\eta = 0.15$

values of s. Actual data, such as presented in Fig. 2, typically require higher values of k.

The derivative of the histogram subset and the detected location of the inflection point is plotted in Fig. 5a for a wafer height $H = 0.225$ and $\eta = 0.1$. Figure 5a is a low noise case, which produces a somewhat sharp secondary peak. Figure 5b shows a higher noise case in which $H = 0.225$ and $\eta = 0.15$ in which the secondary peak is less visible by eye, yet still detectable numerically. There will be other cases discussed later in the article for high η and/or low H in which the inflection point between the secondary and primary peak are not nearly as distinct.

The contact detection algorithm used for this simulation can not directly be used on real-world data, such as the DELIF data displayed in Fig. 2b. The contact detection algorithm is based upon two input parameters, H and η. While it is possible to estimate the noise ratio, η, for a DELIF image based upon camera dark noise measurements, it is nearly impossible to know the vertical position of the wafer relative to the amplitude of the asperity heights, H. For the data displayed in Fig. 2b, the subsection of the histogram used to determine the contact threshold must be determined by visual inspection. In Fig. 2b it is quite clear that there is an inflection point (near Intensity = 125). Using the visually inspected value as an initial estimate for H makes it possible to isolate the appropriate histogram subsection on which to perform the contact analysis described for the simulation. The algorithm described here can then be used to detect the best estimate of contact percentage in the region near the observer's initial estimate.

3 Results and Discussion

Figure 6 is a comparison of the contact percentages calculated from the data histograms as a function of increasing noise ratio and degree of contact. The data in Fig. 6 represent an average contact percentage extracted from simulated noisy images. These noisy images, $Z_{\text{total}}(x, y)$, are created by summing the rough 3D Gaussian surface, $Z_{\text{surface}}(x, y)$, with simulated 3D Gaussian noise image, $Z_{\text{noise}}(x, y)$, (Eq. 6).

$$Z_{\text{total}}(x,y) = Z_{\text{surface}}(x,y) + Z_{\text{noise}}(x,y) \quad (6)$$

Note that $Z_{\text{noise}}(x, y)$ has an associate distribution histogram. The distribution of $Z_{\text{noise}}(x, y)$ is centered at zero and has a standard deviation, σ_2. Each data point in Fig. 6 represents the mean contact calculated for $Z_{\text{total}}(x, y)$ over 10 images, holding $Z_{\text{surface}}(x, y)$ and η constant, but varying $Z_{\text{noise}}(x, y)$. The error bars in Fig. 6 represent the standard deviation of these 10 images.

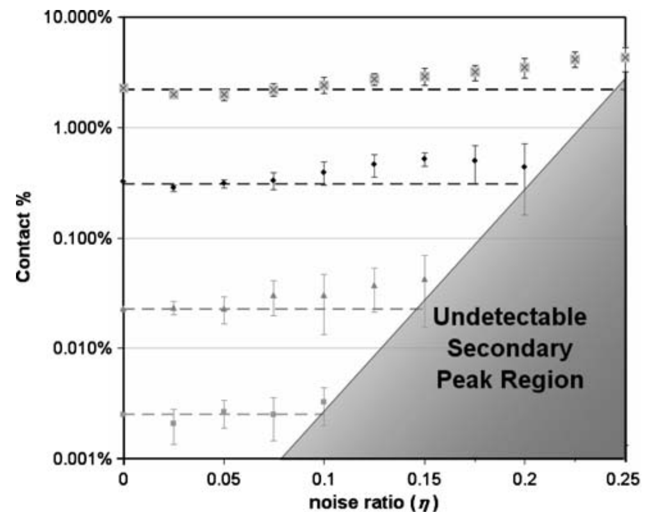

Fig. 6 The measured contact percentages from the simulation (data points with error bars) compared to the *real contact* percentages listed in Table 1 (bold dashed lines) for increasing values of contact and H. ■—$H = 0.075$, ▲—$H = 0.15$, ●—$H = 0.225$, ☒—$H = 0.3$

Figure 6 presents all the simulated data for the cases in which $H > 0$. For the $H = 0$ case, the threshold detection method described earlier yields a minor over prediction of the *real contact* percentage (0.0004% vs. 0%). As discussed earlier, this is an artifact of measurement noise and the discrete nature of the binning process. For $\eta < 0.25$, this small non-zero erroneous contact is at most 0.001%.

For values of $H > 0$, the zero noise cases correctly identifies contact with a slight over-prediction due to the discrete nature of the histogram binning. There is a sharp single-point secondary peak in these histograms when $\eta = 0$, and this secondary peak is only the first point on the left for the entire histogram. The number of pixels counted in this first portion of the contacting side of the histogram is greater than the real number of contacting pixels due the discretization of the bins. For a 500 bin histogram and a wafer height of $H = 0.2$, the contacting bin contains all pixels with heights between $H = 0.200$–0.202. In this case, the *real* number of contacting pixels calculated in Eq. 1 in a 356,352 pixel image is 718 pixels, but the histogram measures 760 contacting pixels, a very minor overprediction.

Zero noise cases are ideal and unrealistic. There will be a small amount of measurement noise even with the best imaging systems. For all cases with low noise ($\eta < 0.1$) and $H > 0$, Fig. 6 shows that the histogram analysis can accurately predict contact. However, as noise increases, the errors in the contact prediction also increase. For high noise cases ($\eta > 0.1$), there is a consistent over-prediction of contact. At high noise values, the secondary peak becomes harder to distinguish. Figure 7 shows the evolution of the shape of the histogram for the contacting surface

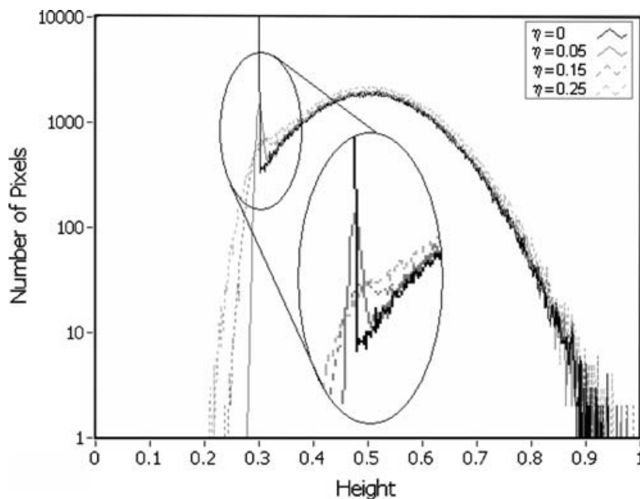

Fig. 7 The effect of increasing measurement noise on the height distribution function for a contacting surface at $H = 0.3$

$H = 0.3$ as a function of noise ratio. Note that the height of the secondary peak decreases and widens as η increases. As the amplitude of the measurement noise increases, the contacting and non-contacting portions of the histogram are blurred together. At high measurement noise ($\eta = 0.25$), the peak becomes nearly undetectable for all simulated values of H. For all *real contact* percentages, there is a critical noise limit that makes contact detection via the histogram method impossible because the contact peak is lost in the noise. The critical noise limit is indicated in Fig. 6 by the shaded region labeled "Undetectable Secondary Peak Region."

Figure 8 shows the histogram subsections analyzed by the threshold detection algorithm and the derivatives for

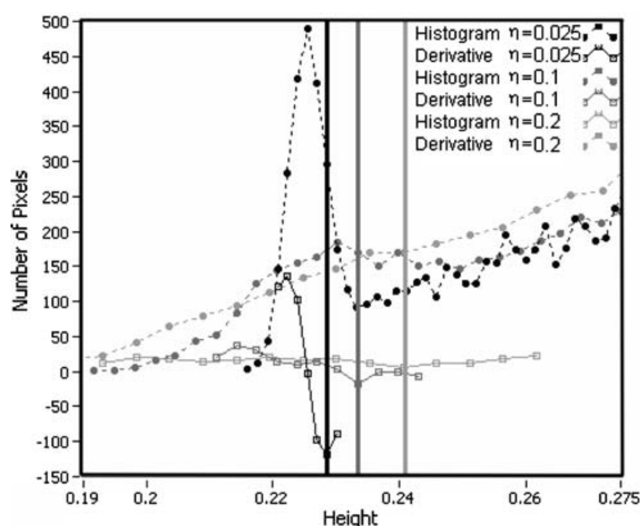

Fig. 8 Contacting peak histogram subsections and their derivatives for $H = 0.225$ at different noise ratio values. The detected contact thresholds are denoted by the solid vertical lines

$H = 0.225$. The detected threshold values and the locations of the minima of the derivatives for each histogram are denoted by the solid vertical lines in Fig. 8. At low noise, $\eta = 0.025$, the peak is sharp and contains few non-contacting pixels. However, the minimum value of the derivative yields a threshold that does not contain the entire peak region. This may be why the contact predictions are on average lower, but still within error of the *real contact* value for $\eta = 0.025$. The histograms still predict contact within $\pm 10\%$ of the *real contact* for this η value. At the noise value $\eta = 0.1$, the detected threshold is just to the right of the peak. It is difficult to discern by eye where the secondary peak ends and the primary peak begins; however, the existence of the secondary peak is evident from the inflection point in the left extreme of the histogram. It is at this noise ratio that the most accurate measurements of contact can be made using the described threshold detection method. Errors in this measurement can be greater than lower noise cases, as high as $\pm 75\%$ of the contact value measured from the histogram.

The precision of the contact measurement increases with increasing contact percentage. This is simply because noise has less effect on stronger signals. When there is a large amount of contact, such as when $H = 0.3$, there are a large number of contacting pixels in the image. Inaccuracies due to histogram bin size and subtle variations in threshold placement have effects similar in magnitude whether $H = 0.075$ or $H = 0.3$. In the $H = 0.075$ and $\eta = 0.025$ case, there are 9 contacting pixels, but the histogram threshold algorithm detects 7 ± 3 pixels over 10 simulated measurement images with varying noise distributions. The resulting error is for this measurement contact measurement is an under-prediction of $22 \pm 33\%$, a low precision prediction. For the $H = 0.3$ and $\eta = 0.025$ case, there are 7807 contacting pixels and the histogram threshold algorithm detects 7036 ± 498 contacting pixels. The resulting error is under-prediction of $10 \pm 7\%$, a more precise measurement due to the fact that there is more contact.

4 Experimental Application: DELIF

The methodology used to calculate contact for this simulation can be used on any experimentally acquired 3D image of two contacting surfaces. High noise ratio values in the range of $\eta > 0.1$ are not typical for a single 12-bit camera imaging system with 4096 gray levels as used in our current DELIF system. A single camera signal may have average signal intensities averaging around 2500 and a standard deviation, $\sigma_1 = 250$. This standard deviation is due primarily to the image contrast resulting from the rough surface profile. The dark noise for that single camera may register at a mean intensity of 230 with a standard

deviation, $\sigma_2 = 12$, which is indicative of measurement noise. Using Eq. 2, we can calculate the noise ratio for this single camera to be $\eta = 0.048$. The intensity in a DELIF image, I_{DELIF}, is actually a result of the ratio of signals from two camera images [16, 17], I^{cam1} and I^{cam2}, shown in Eq. 7.

$$I_{\text{DELIF}} = I^{\text{cam1}} / I^{\text{cam2}} \tag{7}$$

Note that I_{DELIF} is the experimental equivalent of $Z_{\text{total}}(x, y)$ from Eq. 6. The DELIF image has a measurable standard deviation, σ_{DELIF}, or σ_1 in Eq. 2. The division of the two camera images propagates the dark noise from the individual cameras. There is no way to directly measure the dark noise, σ_2, for a DELIF image, but σ_2 can be estimated by dividing the dark noise images, $I_{\text{dn}}^{\text{cam1}}$ and $I_{\text{dn}}^{\text{cam2}}$, then measuring the resulting standard deviation. The intensity for the DELIF dark noise, $I_{\text{DELIF}}^{\text{dn}}$, is calculated in Eq. 8.

$$I_{\text{DELIF}}^{\text{dn}} = I_{\text{dn}}^{\text{cam1}} / I_{\text{dn}}^{\text{cam2}} \tag{8}$$

The noise ratio, η, from Eq. 2, is estimated for a DELIF image, η_{DELIF}, in Eq. 9.

$$\eta_{\text{DELIF}} = \frac{\sigma\left(I_{\text{DELIF}}^{\text{dn}}\right)}{\sigma\left(I_{\text{DELIF}}\right)} \tag{9}$$

This equation does not take into account the increased noise due to camera misalignment. The DELIF images tend to have noise ratios approximately 5 times higher than the individual camera images, $\eta_{\text{DELIF}} = 0.20$–$0.30$. According to Fig. 6, DELIF is incapable of measuring contact percentages below 0.1%. Contact values less than 1% measured by DELIF will tend to have large errors and low precision. DELIF contact measurements greater than 1% contact will be more precise, but less accurate. If this simulation correctly predicts contact calculation errors for DELIF measurements, we have confidence that height distribution histograms of our DELIF images predict the correct order of magnitude of the contact percentage when contact is detectable.

5 Conclusion

We have described a method for detecting contact using 3D optical imaging techniques in which image intensity is a directly correlated to surface height. The precision, accuracy, and errors associated with this contact detection method were evaluated by simulating a measurement image with a Gaussian surface distribution coming into contact with a smooth surface with varying simulated measurement noise. Our specific interest is our ability to use DELIF to quantitatively make contact measurements during CMP, which we have shown we can do to within an order of magnitude.

We have presented contact percentages calculated from histograms with *real contact* percentages spanning 4 orders of magnitude and varying degrees of simulated measurement noise. Contact appears in the histogram as a secondary peak arising in the extreme of the histogram. Introduction of measurement noise into the simulation smoothes and flattens the contact peak. The contact threshold can be determined by seeking the inflection point in the histogram to the right of the secondary peak. This corresponds to the minimum value of the derivative of the histogram. There is a critical noise limit at which the contacting peak in the histogram becomes undetectable. For $\eta = 0.1$ contact of greater than 0.002% is detectable. For $\eta = 0.2$, contact greater than 0.2% is detectable. This critical noise limit is higher with increasing amounts of contact. As noise increases, the error in the contact measurement increases, and this error tends to be smaller for higher contact percentages.

For DELIF images, which have noise ratios, $\eta \sim 0.2$–0.3, we can attain contact percentage measurements using this histogram method for contact percentages greater than approximately 0.1%. Errors are expected to be in the order of $\pm 100\%$. More accurate data can be achieved if a 3D imaging system can be developed that has a low noise-to-signal ratio ($\eta < 0.2$). This technique may also be applied to ex situ interferometric measurements of the rough surface if it permanently deforms after contact. To perform contact analysis on histograms from any 3D imaging technique, this simulation has verified that the asperity height distribution can provide quantitative data about the contacting surface.

Acknowledgments We would like to thank Intel Corp. and Cabot Microelectronics Corp. for funding this project. Thanks also go to Len Borucki of Araca Corp. for his input concerning our DELIF data.

References

1. Cook, L.M.: Chemical processes in glass polishing. J Non-Cryst Solids **120**, 152–171 (1990)
2. Runnels, S.R.: Feature-scale fluid-based erosion modeling for chemical-mechanical polishing. J Electrochem Soc **141**, 1900–1904 (1994)
3. Wu, L.: Analytical model for chemical mechanical polishing of features with different pattern density. J Electrochem Soc **153**, G669–G676 (2006)
4. Muratov, V.A., Fischer, T.E.: Tribochemical polishing. Annu Rev Mater Sci **30**, 27–51 (2000)
5. Steigerwald, J.M., Murarka, S.P., Gutmann, R.J.: Chemical Mechanical Planarization of Microelectronic Materials. Wiley-VCH Verlag GmbH & Co., Weinheim, Germany (2004)
6. Mahajan, U., Bielmann, M., Singh, R.K.: Dynamic lateral force measurements during chemical mechanical polishing of silica. Electrochem Solid-State Lett **2**, 80–82 (1999)

7. Das, T.K., Ganesan, R., Sikder, A.K., Kumar, A.: Online end point detection in CMP using SPRT of wavelet decomposed sensor data. IEEE Trans Semicond Manuf **18**, 440–447 (2005)
8. Kim, H., Jeong, H., Lee, E., Shin, Y.: Pad surface characterization and its effect on the tribological state in chemical mechanical polishing. Adv Abrasive Tech VI Key Eng Mater **257–258**, 383–388 (2004)
9. Paul, E.: A model of chemical mechanical polishing. J Electrochem Soc **148**, G355–G358 (2001)
10. Pau, M., Aymerich, F., Ginsu, F.: Ultrasonic measurements of nominal contact area and contact pressure in a wheel-rail system. Proc Inst Mech Eng **214**, 231–243 (2000)
11. Glovnea, R.P., Forrest, A.K., Olver, A.V., Spikes, H.A.: Measurement of sub-nanometer lubricant films using ultra-thin film interferometry. Tribol Lett **15**, 217 (2003)
12. Muldowney, G.P., Elmufdi, C.L.: The impact of pad microtexture and material properties on surface contact and defectivity in CMP. CMP-MIC Proc **11**, 262–271 (2006)
13. Gray, C., Rogers, C., Manno, V.P., White, R., Moinpour, M., Anjur, S.: Determining pad-wafer contact using dual emission laser induced fluorescence. In: Materials Research Society Symposium Proceedings, vol. 991. Materials Research Society, Warrendale, PA (2007)
14. Elmufdi, C.L., Muldowney, G.P.: The impact of diamond conditioning on surface contact in CMP pads. In: Materials Research Society Symposium Proceedings, vol. 991. Materials Research Society, Warrendale, PA (2007)
15. Lawing, A.S.: Pad conditioning and removal rate in oxide chemical mechanical polishing. In: Proceedings of the 5th International Symposium on CMP, pp. 1–8. The Electrochemical Society, Pennington, NJ (2002)
16. Coppeta, J., Rogers, C.: Dual emission laser induced fluorescence for direct planar scalar behavior measurements. Exp Fluids **25**, 1–15 (1998)
17. Hidrovo, C.H., Hart, D.P.: Emission reabsorption laser induced fluorescence (ERLIF) film thickness measurement. Meas Sci Technol **12**, 467–477 (2001)
18. Gray, C., Apone, D., Rogers, C., Manno, V.P., Barns, C., Moinpour, M., Anjur, S., Philipossian, A.: Viewing asperity behavior under the wafer during CMP. Electrochem Solid State Lett **8**, G109–G111 (2005)
19. Lin, Y.Y., Lo, S.P.: A study of a finite element model for the chemical mechanical polishing process. Int J Adv Manuf Technol **23**, 644–650 (2004)